applied nano

MDPI

Article

Structure–Optical Properties and Sustainability Assessment of Carbon Dots Derived from *Laurus nobilis* Leaves

Valeria De Matteis [1,*], Cristina Baglivo [2], Silvia Tamborino [2], Mariafrancesca Cascione [3], Marco Anni [3], Paolo Vitali [4], Giuseppe Negro [5], Mariaenrica Frigione [2], Paolo Maria Congedo [2] and Rosaria Rinaldi [3]

[1] Department of Experimental Medicine (DiMeS),University of Salento Centro Ecotekne, Via Monteroni, 73100 Lecce, Italy
[2] Department of Engineering for Innovation (DII), Campus Ecotekne, University of Salento, Via Monteroni, 73100 Lecce, Italy; cristina.baglivo@unisalento.it (C.B.); silvia.tamborino@unisalento.it (S.T.); mariaenrica.frigione@unisalento.it (M.F.); paolo.congedo@unisalento.it (P.M.C.)
[3] Department of Mathematics and Physics "E. De Giorgi", University of Salento, Via Monteroni, 73100 Lecce, Italy; mariafrancesca.cascione@unisalento.it (M.C.); marco.anni@unisalento.it (M.A.); ross.rinaldi@unisalento.it (R.R.)
[4] Radice Cubica s.r.l, Via Delle Bombarde 14, 73100 Lecce, Italy; info@radicecubica.com
[5] ASCLA Società Cooperativa Impresa Sociale, Via Sesia 17, 73042 Casarano, Italy; info@ascla.it
* Correspondence: valeria.dematteis@unisalento.it

Abstract

Carbon dots (CDs) derived from renewable biomass are emerging as sustainable alternatives to traditional nanomaterials for applications in bioimaging, sensing, and photonics. In this study, we reported a one-step synthesis of photoluminescent CDs from *Laurus nobilis* leaves particularly spread in the Mediterranean area. The resulting nanoparticles (NPs) exhibited average diameters of 3–5 nm and high colloidal stability in water. Structural analysis by X-Rays Diffraction revealed the presence of amorphous graphitic domains, while infrared spectroscopy confirmed oxygenated functional groups on the CD surface. Spectrofluorimetric analysis showed excitation-dependent blue–green emission with a maximum at 490 nm that can be applied also as label agents for cells. The environmental sustainability of the synthetic procedure was evaluated through a Life Cycle Assessment (LCA), highlighting that the current impacts were primarily associated with electricity consumption, due to the laboratory-scale nature of the process. These impacts are expected to decrease significantly with future scale-up and process optimization.

Keywords: C-dots; *Laurus nobilis*; physico-chemical properties assessment; life cycle assessment

Academic Editors: David Marrero-López and Christian Julien

Received: 30 June 2025
Revised: 22 August 2025
Accepted: 25 August 2025
Published: 2 September 2025

Citation: De Matteis, V.; Baglivo, C.; Tamborino, S.; Cascione, M.; Anni, M.; Vitali, P.; Negro, G.; Frigione, M.; Congedo, P.M.; Rinaldi, R. Structure–Optical Properties and Sustainability Assessment of Carbon Dots Derived from *Laurus nobilis* Leaves. *Appl. Nano* **2025**, *6*, 19. https://doi.org/10.3390/applnano6030019

Correction Statement: This article has been republished with a minor change. The change does not affect the scientific content of the article and further details are available within the backmatter of the website version of this article.

1. Introduction

CDs represent an emerging class of zero-dimensional carbon-based nanomaterials, typically exhibiting lateral dimensions below 10 nm [1]. Structurally, CDs are composed of a disordered or partially graphitized carbonaceous core, surrounded by a heterogeneous shell enriched with oxygenated functional groups—such as hydroxyl, carboxyl, and carbonyl moieties—which play a crucial role in modulating surface reactivity, colloidal stability, and emissive behavior [2,3]. In addition, the versatility of carbon—an earth-abundant element capable of forming sp, sp^2, and sp^3 hybridized atoms—enables the formation of nanostructures Their unique combination of tunable photoluminescence, high aqueous dispersibility, outstanding chemical stability, and inherently low cytotoxicity has positioned them at the forefront of advanced applications in bioimaging, fluorescent sensing, photocatalysis, energy storage, and optoelectronic devices [4–6] with tunable optoelectronic

properties [7]. The photoluminescent behavior of CDs is influenced by a combination of quantum confinement, edge effects, and surface defect states. These properties can be modulated by the synthetic strategy and the nature of the carbon precursor [8]. The development of green synthesis routes is essential to support the large-scale deployment of CDs in environmental and energy applications [9].

CDs are classified based on the structure of their carbon core and the nature of their surface functional groups. The main types include graphene quantum dots (GQDs), carbon quantum dots (CDs), carbon nanodots (CNDs), and carbonized polymer dots (CPDs). GQDs are small, anisotropic fragments of graphene that can form single or multiple layers, and they exhibit quantum confinement and edge effects due to chemical functionalities located at their edges or within interlayer defects. CDs, in general, display intrinsic luminescence and quantum confinement effects because of their nanocrystalline structure and surface chemical groups [10]. CNDs are highly carbonized particles that exhibit strong edge effects but do not possess crystalline or polymeric structures, and they do not show quantum confinement phenomena. CPDs, on the other hand, are composed of a carbonized core surrounded by polymer chains and various functional groups, combining carbonization with polymeric characteristics. These structural and chemical features are crucial in determining the optical and functional properties of each type of CD [11].

In recent years, a major thrust in CDs research has shifted toward the development of environmentally benign and cost-effective synthesis routes, in alignment with the principles of green chemistry and circular economy. This is because the synthesis of these materials often requires highly energy-consuming techniques and complex instrumentation using bottom-up or top-down approaches [12]. In this context, the valorization of renewable biomass—particularly agri-food waste streams—has emerged as a compelling alternative to traditional synthetic methods, offering abundant carbon sources naturally enriched in heteroatoms (e.g., N, S, O) and aromatic systems conducive to in situ doping and enhanced carbonization efficiency [13]. These routes drastically reduce the need for toxic reagents or high-temperature treatments typical of bottom-up synthetic methods [14–17]. *Laurus nobilis* pruning residues represent an underutilized biomass stream rich in phenolic compounds, lignin, and terpenoids [18]. In this study, we presented a reproducible synthesis of CDs by one-pot carbonization of *Laurus nobilis* leaves biomass in aqueous solution and microwaves, obtaining photoluminescent NPs without the need for external dopants or passivating agents. This method was reported in previous works.

For example, wild lemon leaves were used as starting biomass. They were crushed, suspended in hot water, and stirred, after which the resulting solution was subjected to microwave irradiation with periodic cooling. Following filtration, centrifugation, and dialysis, a clear solution of carbon dots was obtained, exhibiting bright green-blue fluorescence under UV light, confirming the formation of CDs [19]. Suhail et al. [20] used Carrageenan as precursor to prepare CDs via microwave-assisted synthesis using a microwave oven The solution containing biomass was subjected to multiple short cycles of 15 s by microwave irradiation.

Sharma et al. [21] synthesized CDs from *Calotropis gigantea* leaf extract using a microwave-assisted method. The powdered leaves were mixed with distilled water and then processed in a 900 W domestic microwave until a brown viscous fluid formed.

Yu et al. [22] used phthalic acid (naturally present in *Papaver somniferum* and *Cocos nucifera*) and triethylenediamine hexahydrate with different feed ratio. The solution was placed at the center of the rotation plate of a domestic microwave oven (700 W) and heated for 60 s in order to obtain fluorescent CDs with similar sizes in the range of 2–6 nm. CDs can also be obtained from glycine The CDs were prepared by microwave heating of glycine naturally contained in some foods, using household microwave oven (800 W) for

3 min [23]. In another work, CDs were synthesized from fresh Mexican Mint leaves using a microwave-assisted reflux method. The leaves were thoroughly cleaned, ground with distilled water, and the resulting extract was subjected to microwave irradiation for varying durations (4, 5, 6, and 7 min) obtaining spherical nanomaterials in shape with a particle size of 2.43 ± 0.02 nm [24].

Using our method, we obtain CDs exhibited average diameters of 3–5 nm. These nanomaterials were deeply characterized to understand their physico-chemical properties following the LCA on synthetic procedure. This was performed to assess its environmental performance and investigate the potential advantages and limitations of producing CDs from waste materials on a laboratory scale. The LCA methodology makes it possible to objectively quantify the environmental impacts associated with a product or service, from raw material extraction to final disposal. Particularly in chemistry and emerging technologies, LCA is a crucial tool for comparing the sustainability of new products against those already on the market [25].

However, the analysis of laboratory-scale processes presents significant challenges. As highlighted by Piccinno et al. [26], the use of laboratory-scale data in environmental assessments often leads to an overestimation of impacts when compared to commercially available materials. This discrepancy arises from the fact that industrial processes benefit from optimization and scale effects, which improve material and energy efficiency. Consequently, such comparisons may not accurately reflect the true potential of the newly developed material or process. Performing a scale-up is therefore essential to enable a more realistic and meaningful comparison with existing technologies at the commercial level

2. Materials and Methods

2.1. Synthesis of CDs

The synthesis of CDs was carried out as follows: *Laurus nobilis* leaves provided by the company Radice Cubica s.rl, Lecce, Italy, were thoroughly washed to remove dust and pollutants. They were then air-dried at room temperature, chopped, and 3 g were weighed and placed into a glass flask with 20 mL of ultrapure water. The glass flask was then placed in a microwave oven for approximately 3 min at maximum power. Afterward, the solution was transferred into centrifuge tubes and centrifuged at 10,000 rpm for 30 min. The dark brown pellet containing the synthesized nanoparticles was collected and washed with deionized water.

The pellet was collected and dried in an oven at 40 °C for 24 h to eliminate all organic residues. A graphical representation of the synthesis was shown in Figure 1.

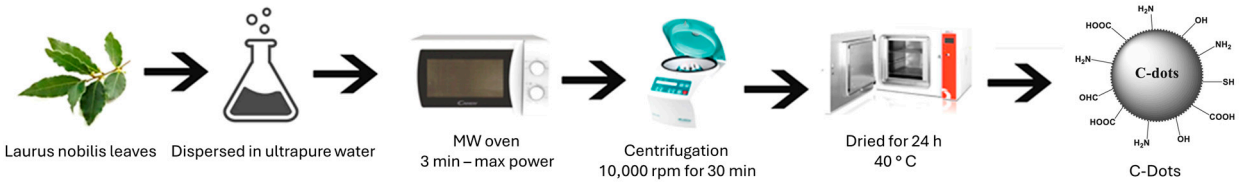

Figure 1. Schematic representation of CDs synthetic route.

2.2. Characterization of CDs

Transmission Electron Microscopy (TEM) images were acquired using a JEOL 2100 equipped with a CCD camera Orius SC2001 from Gatan operating at 120 kV. The nanoparticle (NP) suspensions were drop-cast onto standard carbon-coated 400-mesh copper grids and dried prior to imaging. Dynamic Light Scattering (DLS) and ζ-potential measurements were carried out in aqueous solution (25 °C, pH 7) using a Zetasizer Nano-ZS (ZEN3600, Malvern Instruments Ltd., Malvern, UK) equipped with a 4.0 mW He–Ne laser operating

at 633 nm. The nanoparticle size distribution was determined by analyzing 100 individual carbon dots (CDs) from TEM images, and the data were fitted using a Gaussian function. UV–Vis absorption spectra were recorded using a Shimadzu UV-2550 spectrophotometer with 1 cm path length quartz cuvettes. Fourier-transform infrared (FTIR) spectra of the NPs were acquired in the 400–4000 cm^{-1} range at a resolution of 4 cm^{-1} using a Jasco-670 Plus spectrometer (Jasco, Tokyo, Japan). Photoluminescence (PL) measurements were performed in aqueous solutions using a continuous-wave diode laser with an excitation wavelength of 405 nm and a maximum power output of 20 mW. The emission spectra were recorded with a Spectral Products SM442 CCD spectrometer with a spectral resolution of 0.6 nm. X-ray diffraction (XRD) analysis was conducted in Bragg–Brentano reflection geometry using filtered Cu-Kα radiation. Data were collected over a 2θ range of 20–80° with a step size of 0.02° per second.

2.3. Cell Culture

Human breast cancer cells (MCF-7, ATCC HTB-22™) were cultured in Dulbecco's Modified Eagle Medium (DMEM; Sigma-Aldrich, Dorset, UK) supplemented with 2 mM L-glutamine, 100 U/mL penicillin–streptomycin (Sigma-Aldrich, Dorset, UK), and 10% (*v*/*v*) fetal bovine serum (FBS; Sigma-Aldrich, Dorset, UK). Cells were maintained in a humidified incubator at 37 °C in an atmosphere containing 5% CO_2.

2.4. Confocal Images

Laser scanning confocal microscopy was performed using a Zeiss LSM700 confocal system (Zeiss, Oberkochen, Germany) equipped with an Axio Observer Z1 inverted microscope and a 100 × oil immersion objective lens (NA 1.46). Image acquisition and processing were carried out using ZEN 2010 software (Zeiss). For confocal analysis, MCF-7 cells (6.2×10^4 cells per dish) were seeded in 50 × 7 mm glass-bottom Petri dishes (WillCo Wells B.V., Amsterdam, The Netherlands). After 24 h, the cells were incubated with carbon dots (C-dots) at a concentration of 1 μg/mL for an additional 24 h. Cells were then washed with phosphate-buffered saline (PBS; Sigma-Aldrich, Dorset, UK), fixed with 0.25% glutaraldehyde (Sigma-Aldrich, Dorset, UK) for 20 min at room temperature, and permeabilized with 0.1% Triton X-100 (Sigma-Aldrich, Dorset, UK) for 5 min. Images were acquired using the ATTO 488 laser line for excitation.

2.5. Life Cycle Assessment (LCA)

To assess the environmental impact of the CDs produced from *Laurus nobilis* leaves, an LCA study was carried out using the SimaPro 10.2 Software [27]. The analysis uses the production of 1 kg of CDs as the functional unit, and the system boundaries follow a "cradle-to-gate" approach. This means that all life cycle stages, from raw material supply to the point where the final product leaves the production site, are included. The latter stages, such as application (e.g., in electrodes), use phase, and end-of-life, are not considered. Transport phases are also excluded, assuming the raw material comes from local sources, and to keep the focus on the production process.

Environmental impacts were assessed using the ReCiPe 2016 Endpoint (H) method, which evaluates damage at the endpoint level. This helps to interpret the results by grouping them into three main areas of protection: human health, ecosystem, and resource. The impact categories analysed include climate change, human toxicity, fossil resource depletion, terrestrial ecotoxicity, and land use. These categories were selected because they are particularly relevant to the life cycle of the studied system.

The study is based on data representative of the Italian context in 2025.

2.5.1. Life Cycle Inventory (LCI)

The data used in the study include both primary and secondary data depending on the stage of analysis considered. The laurel leaves used in this study come from the essential oil extraction chain. After the steam distillation process, they are no longer suitable for food consumption and must therefore be disposed of. Since this is a waste with no economic value, and in accordance with the recommendations of ISO 14044, which recommends avoiding allocation procedures [28], these leaves were included in the system under study with zero environmental load.

A critical aspect in laboratory-scale LCA analysis concerns the correct quantification of energy consumption of the instrumentation used. Since small quantities of material are often processed, attributing total energy consumption to them can lead to a significant overestimation of impact. For this reason, a weighted energy allocation criterion was adopted, assuming that the instrumentation is filled and distribute consumption over the entire theoretical capacity per cycle. This approach provides more realistic energy estimates, facilitating more reliable comparisons.

2.5.2. Microwaves Oven

To calculate the energy consumption associated with microwave use, it was assumed that 6 test tubes with a maximum capacity of 85 mL were placed inside, corresponding to the maximum capacity of the centrifuge that is used next. Each test tube was assumed to contain 6 g of leaves and 40 mL of water (corresponding to 2 times the doses used in experimentation), for a total of about 46 g of solution per tube (versus the original 23). The total amount processed per cycle is 276 g.

The total energy consumption calculated as the product of power and operating time was 0.035 kWh. By dividing the energy value obtained by the total mass processed, a specific energy consumption of about 0.000127 kWh per gram of solution is obtained. Finally, relating this data to the actual reference quantity, consisting of 3 g of leaves and 20 mL of water (23 g), we estimate an energy consumption of about 0.00292 kWh.

2.5.3. Centrifugation Process

For the centrifugation process, on the other hand, it was more complicated, since the centrifuge was operated at less than the maximum number of revolutions per minute, calculating power consumption considering the rated power would have been an overestimate. Therefore, power consumption was estimated based on the number of revolutions per minute.

The centrifuge was operated at 10,000 rpm for 30 min. To estimate the power absorbed by the centrifuge during operation at 10,000 rpm, the cubic law was applied, according to which the power required by a centrifugal load varies proportionally to the cube of the speed ($P \propto rpm^3$). Assuming a power of 2.5 kW (208 V, 12 A) at 30,000 rpm, the theoretical power related to rotation at 10,000 rpm alone results:

$$P_{rot} = 2.5\ kW \times \left(\frac{10{,}000}{30{,}000}\right)^3 = 92.6\ W \quad (1)$$

However, for a more realistic estimate of power consumption, it is also necessary to consider base power, independent of rotational speed, attributable to the electronic, control and cooling systems. This has been estimated at 10% of the rated power, or 250 W. Therefore, the total estimated power at 10,000 rpm is

$$P_{tot} = P_{base} + P_{rot} = 250\ W + 92.6\ W = 342.6\ W \quad (2)$$

Thus, considering these powers, the consumption is 0.1713 kWh. This was then allocated by assuming to totally fill the centrifuge with 6 tubes of 46 g of solution each, for a total solution mass of 276 g and a consumption per unit mass of 0.000621 kWh/g. For the experimental unit mass of 23 g, the consumption is therefore 0.0142 kWh.

2.5.4. Oven

The nominal power rating of the oven is 1.2 kW, but by operating at much lower temperatures than the maximum power rating, the actual energy consumption is lower.

Assuming that the oven power is proportional to the operating temperature, and considering a maximum temperature of 230 °C, the estimated power at 40 °C is 0.21 kW.

The oven has a volumetric capacity of 56 L, so 108 tubes per cycle (arranged in 3 levels of 36 tubes, respectively), each containing 6 g of leaves and 40 mL of water, were considered to fill it. The total amount treated in one cycle is therefore about 4.968 kg. Specific energy consumption was calculated by dividing the total energy consumption by the total mass treated, yielding a value of about 0.00101 kWh/g of treated solution. For 23 min, an energy consumption of about 0.0232 kWh is obtained.

These integrated estimates represent a reasonable compromise, providing greater transparency and repeatability in the context of a laboratory-scale LCA evaluation.

Input and output data are shown in Table 1.

Table 1. Inputs and Outputs to produce 55 mg of CDs from *Laurus nobilis*.

Laurus nobilis				
	Unite of Measure	**Quantity**	**Data**	**Comment**
Input				
[DUMMY] Recycled waste, unspecified	g	3	I	*Laurus nobilis* Leaves
Water, ultrapure {RER} | market for water, ultrapure | Cut-off, S	g	20	I	
Tap water {RER} | market group for tap water | Cut-off, S	g	500	I	Wash Water
Electricity, medium voltage {IT} | market for electricity, medium voltage | Cut-off, S	kWh	0.00292	II	Microwaves Oven Midea MM720CTB; 700 W; 3′
Electricity, medium voltage {IT} | market for electricity, medium voltage | Cut-off, S	kWh	0.0142	II	Centrifuge Beckman Coulter Allegra 64R; 208 V; 12 A; 10,000 rpm; 30′
Electricity, medium voltage {IT} | market for electricity, medium voltage | Cut-off, S	kWh	0.0232	II	Oven; 56 L; 1.2 kW; 40 °C for 24 h
Output				
Wastewater, unpolluted {RoW} | treatment of wastewater, unpolluted, wastewater treatment | Cut-off, S	L	0.51	II	Wash water + supernatant
Laurus nobilis CDs	mg	200	I	

3. Results and Discussion

The TEM image showed nearly spherical, well-dispersed NPs with high density. The uniform contrast suggested a homogeneous carbon core; the 100 nm scale bar indicated individual diameters of only a few nanometers. The absence of aggregation highlights good colloidal stability, likely due to hydrophilic surface functional groups on the CDs (Figure 2a). The histogram showed a population centered around ~4 nm with a relatively narrow size spread (ranging from 2 to 6 nm); the red Gaussian fit aligned well with the data, confirming a quasi-monodisperse distribution and a low polydispersity index (Figure 2b).

Such small sizes were typical of CDs synthesized via bottom-up approaches and it is suitable for both quantum fluorescence and interactions with polymeric or biological systems. The absorbance spectrum where it was depicted an intense peak at 270–280 nm with a slight extension into the visible region was reported. This peak can be attributed to n-π* transitions of carbonyl groups (–C=O) and π-π* transitions of carbon–carbon double bonds (–C=C). The solid line represents the freshly prepared CDs, while the dashed line showed the UV–Vis spectrum after 96 h. The minimal shift and retention of peak intensity suggested excellent temporal stability, with the CDs maintaining their optical properties over time (Figure 2c).

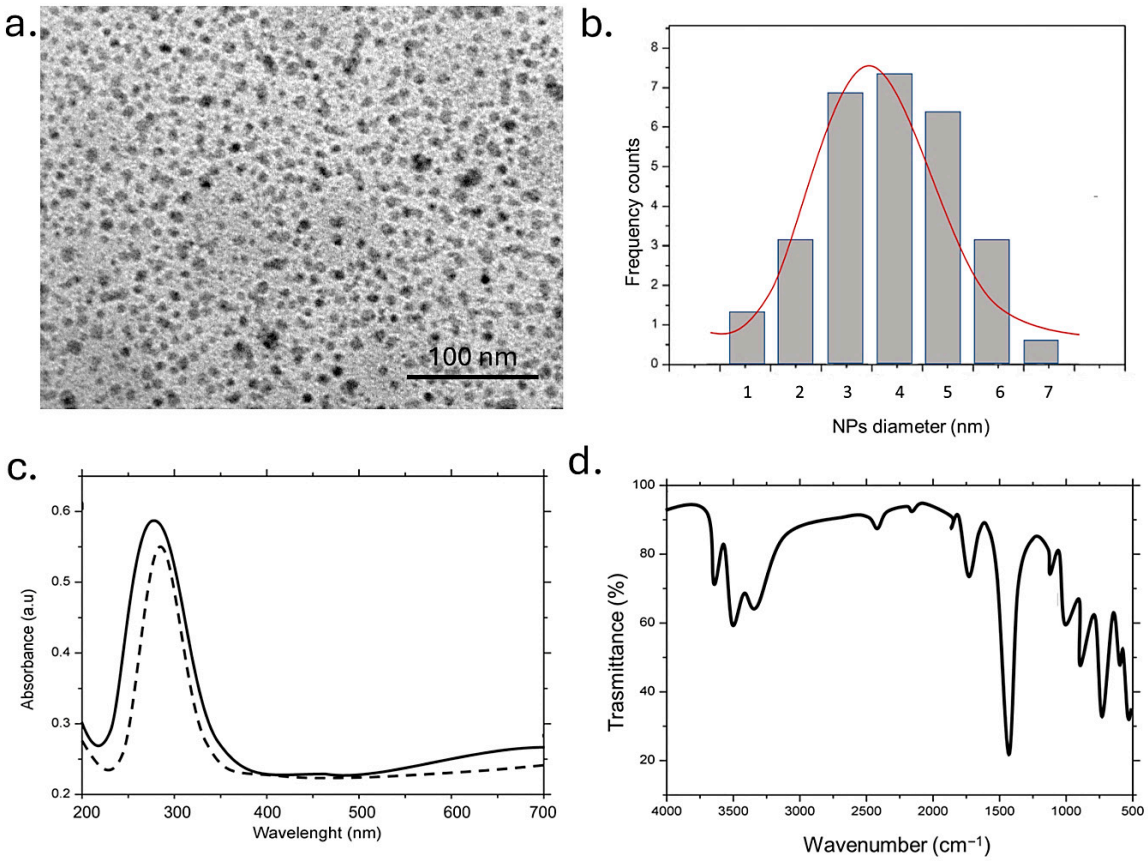

Figure 2. Representative TEM image of CDs (**a**) and (**b**) statistical analysis with Gaussian fit (black line) (**c**). UV-vis of CDs immediately after synthesis (black line) and after one week (dashed line); (**d**) and FTIR measurements.

In the FTIR spectra several characteristic peaks were observed. A broad band in the 3400–3200 cm^{-1} region was attributed to overlapping O–H and N–H stretching vibrations. The peak around 3400 cm^{-1} was typically associated with hydroxyl groups, while the signal near 3300–3200 cm^{-1} could indicate the presence of primary or secondary amine groups. These functionalities are likely derived from polyphenols, flavonoids, tannins, and amino acids naturally present in the *Laurus nobilis* leaves.

They were responsible for the high hydrophilicity of the CDs inducing good water dispersibility. The peaks observed in the 1650–1550 cm^{-1} range were consistent with C=O/C=C and C–N stretching vibrations, which may be indicative of amide bonds or conjugated graphitic domains. These features could originate from interactions between amine and carbonyl groups naturally present in the extract or could have formed during subsequent synthesis or processing steps. The C–N stretching band at 1380 cm^{-1} further confirmed the presence of amine functionalities. Finally, signals in the 1100–1000 cm^{-1}

range were attributed to C–O–C vibrations, typical of oxidized epoxide or ether groups^{-1}. The last signals indicated a certain degree of oxidation of the precursor molecules, contributing to reactive surface functionalities suitable for further chemical modification (Figure 2c).

DLS measurements on CDs in water confirmed the TEM data and showed NPs with a hydrodynamic radius of (3 ± 3) nm A negative surface charge was observed (−30 ± 3) mV and (−30 ± 5) mV indicated a good colloidal stability (Table 2).

Table 2. DLS and ζ-potential measurements on freshly prepared CDs in water.

Dynamic Light Scattering (DLS)	Zeta Potential
3 nm ± 1	−30 mV ± 5

The optical and structural characterization of the synthesized CDs confirmed their successful formation and revealed features consistent with amorphous, fluorescent carbon-based nanomaterials. As shown in Figure 3a, the fluorescence emission spectrum displayed a broad and intense peak centered around 510 nm when excited under UV light (laser 405 nm, 20 mW power), indicating strong visible-range photoluminescence. The observed emission profile, with its wide full width at half maximum (FWHM), was indicative of a heterogeneous distribution of emissive sites or surface states, which is a common characteristic of CDs derived from green or biomass-based precursors [29]. The visual confirmation of this luminescence was provided by the inset photographs, where the aqueous CDs suspension exhibited a pale-yellow color under ambient light and a bright blue-green fluorescence under UV illumination (365 nm) [30]. This behavior confirmed the effective incorporation of optically active functional groups or passivating agents on the surface of the CDs. Indeed, the surface of the CDs hosts a variety of optically active functional groups, originating both from the carbonaceous precursors and from functionalization treatments. These groups modulate the distribution of electronic energy levels and act as active sites for photon emission. Hydroxyl and carboxyl groups enhance hydrophilicity and may introduce surface electronic states that act as electron traps, thereby modulating the emission wavelength. Amino groups, on the other hand, have an electron-donating effect and promote blue emission. In the case of natural or biomass-derived precursors—such as *Laurus nobilis* leaves—the functional groups introduced are largely oxygenated, such as –OH and –COOH, but may also include aromatic heterocycles and traces of phenolic groups, depending on the chemical composition of the starting material. To evaluate their potential as fluorescent agents, we incubated breast cancer cells (MCF-7) with the CDs at a concentration of 1 μg/mL for 24 h. As shown in Figure 3b, the labeled cells exhibited a markedly higher fluorescence compared to the control group, clearly indicating their promising applicability in nanomedicine. Complementary structural analysis was conducted via X-Ray Diffraction (XRD) (Figure 3b). The diffraction pattern reveals a broad, featureless peak centered around $2\theta = 21^{\circ}$, corresponding to the (002) plane of graphitic carbon. The absence of sharp crystalline peaks confirms the predominantly amorphous nature of the synthesized CDs, indicating the presence of disordered carbon domains with enlarged interlayer spacing compared to crystalline graphite. Such a structural arrangement is typically observed in nanocarbons obtained under mild hydrothermal or microwave-assisted conditions, particularly when natural precursors are employed. The amorphous character is also consistent with the abundant surface functional groups introduced during the synthesis, which play a key role in determining solubility, stability, and surface reactivity. This is in good agreement with previous literature [31–33].

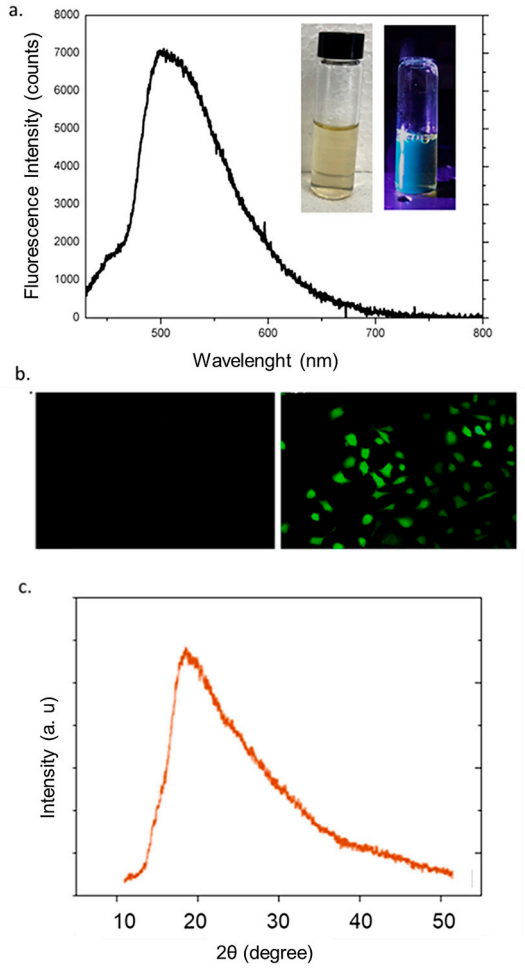

Figure 3. Florescence measurements (**a**); representative confocal analysis of fixed MCF-7 cells (left) untreated and (right) treated with 1 μg/mL for 24 h of CDs (scale bar 10 μm) (**b**); XRD pattern of CDs (**c**).

Life Cycle Impact Assessment (LCIA)

The environmental impacts are presented in Figure 4, aggregated into the three end-point categories: Human Health, Ecosystem, and Resources. The results show that the largest impact is attributable to energy consumption. For human health, it accounts for about 90% of the total impact, with tap and ultrapure water contributing an additional 10%. In the ecosystem area, electricity remains the main source of impact, though wastewater treatment provides a small environmental credit. Resource depletion is almost entirely driven by electricity, with negligible input from ultrapure water.

However, these results should not be interpreted as indicative of the unsustainability of the process, as they largely reflect the operating conditions of a system still confined to the laboratory scale. Although normalization criteria have been adopted to account for this limitation, it is reasonable to assume that moving to a pilot scale, and subsequently to industrial production, may lead to a substantial optimization of energy efficiency and a consequent reduction in environmental impact, as process scale-up typically enables improved material and energy performance through optimized operations and economies of scale [25]. This assumption is further supported by empirical data from the analysis of 25,000 industrial sites across Europe and the U.S., which revealed a consistent inverse correlation between production-specific energy consumption and production capacity: larger facilities systematically show lower specific energy consumption across multiple sectors and regions [34]. For this reason, future LCA studies on larger-scale systems will be

important to improve impact estimates and allow fair comparisons with similar commercial products. Until the process becomes more technologically mature, direct comparisons with existing market alternatives would be premature and possibly misleading. Nonetheless, the LCA results presented here provide a first quantitative basis that may support environmental certification and eco-labelling efforts in future developments, once the process is scaled up and stabilized.

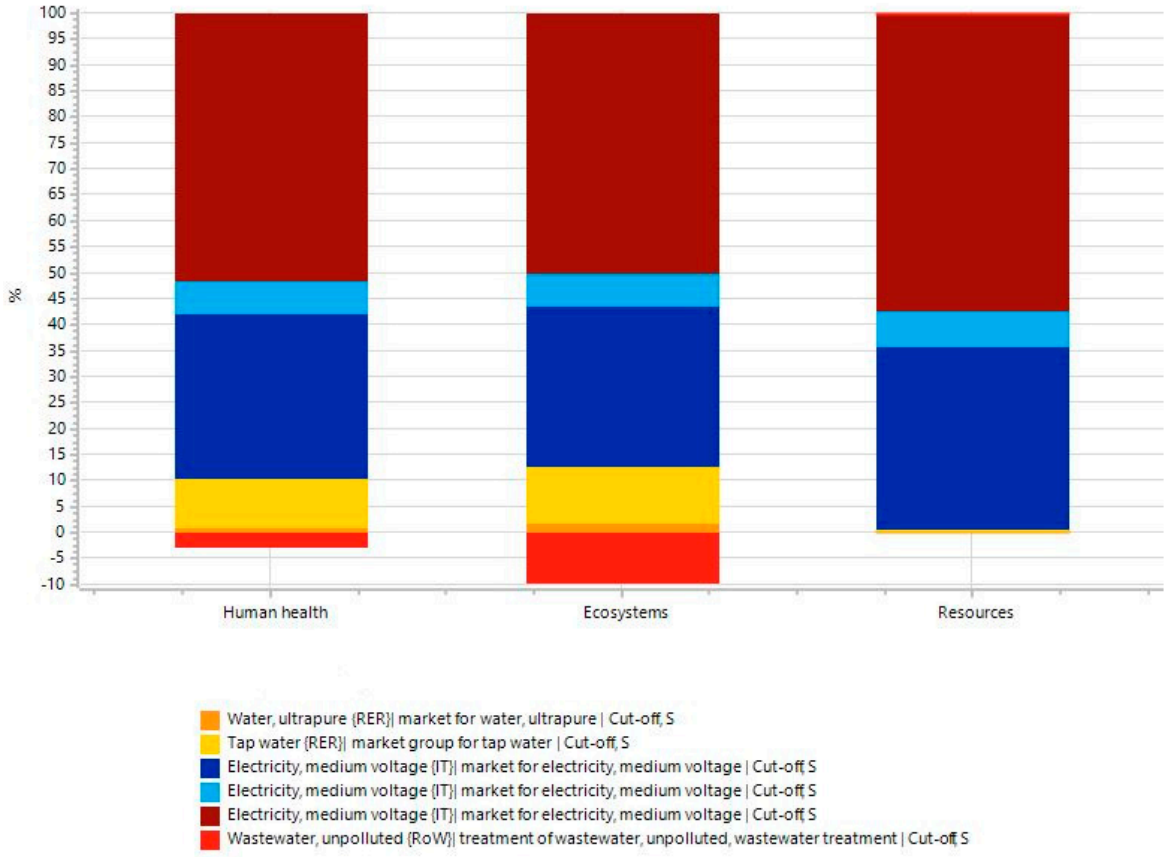

Figure 4. Aggregated results of the endpoint LCA (ReCiPe 2016 H/A) to produce 1 kg of CDs from *Laurus nobilis*.

4. Conclusions

In this study, we successfully demonstrated the green synthesis of CDs from *Laurus nobilis* leaves via a one-step method, yielding photoluminescent NPs with average diameters of 3–5 nm and excellent colloidal stability in aqueous media. Structural and spectroscopic analyses confirmed the presence of amorphous graphitic domains and surface oxygenated functional groups, which contribute to the observed excitation-dependent blue–green fluorescence. These features made the obtained CDs promising candidates for bioimaging and sensing applications, without the need for additional passivating or doping agents. Importantly, we integrated a LCA to preliminarily evaluate the environmental sustainability of the proposed synthetic route. Although current environmental impacts are mainly attributed to electricity consumption typical of laboratory-scale operations, the analysis suggests that these impacts could be significantly reduced through process scale-up and optimization. It is important to note that this study adopts the ReCiPe 2016 Endpoint (H) methodology, which provides aggregate impact scores expressed in normalized units (Pt) or expressed as a percentage of the total impact. While this approach allows for immediate interpretation of environmental damage, specific impact categories, such as Global Warming Potential (GWP), are not directly expressed in easily comparable units such as

kg CO_2 equivalent. Future studies on a larger scale could use the ReCiPe 2016 Midpoint method to enable comparisons based on common indicators, facilitating benchmarking with commercial alternatives. This work not only underlines the potential of agri-food residues, such as *Laurus nobilis* pruning waste, as valuable carbon sources for nanomaterial synthesis, but also emphasizes the importance of embedding sustainability assessments early in the development of novel materials. Overall, the combination of renewable biomass valorization, straightforward synthesis, and integration of environmental evaluation frameworks positions this approach as a promising step toward the scalable and sustainable production of carbon-based nanomaterials for future technological applications.

Author Contributions: V.D.M.: conceptualization, methodology, writing—original manuscript, M.C., C.B., S.T. and M.A.: software, data analysis, methodology, editing—original manuscript, P.V. and G.N.: methodology, M.F., P.M.C. and R.R.: supervised and edited the work. All authors have read and agreed to the published version of the manuscript.

Funding: This research received no external funding.

Data Availability Statement: The original contributions presented in this study are included in the article. Further inquiries can be directed to the corresponding author.

Acknowledgments: Project "BOtanical REsources for ALternative battEries" (acronym "BO.RE.AL.E."), within the framework of the PNRR (National Recovery and Resilience Plan), Mission 4 "Education and Research"—Component 2 "From Research to Business"—Investment Line 1.4 "Enhancement of research infrastructures and creation of national R&D champions in key enabling technologies"—Research and Development Program "National Research Centre for Agricultural Technologies—AGRITECH", CN 00000022—SPOKE 8—CUP: J73C24000260003.

Conflicts of Interest: The authors declare that they have no commercial or financial conflicts of interest related to this work.

References

1. Mkhari, O.; Ntuli, T.D.; Coville, N.J.; Nxumalo, E.N.; Maubane-Nkadimeng, M.S. Supported carbon-dots: A review. *J. Lumin.* **2023**, *255*, 119552. [CrossRef]
2. Georgakilas, V.; Perman, J.A.; Tucek, J.; Zboril, R. Broad Family of Carbon Nanoallotropes: Classification, Chemistry, and Applications of Fullerenes, Carbon Dots, Nanotubes, Graphene, Nanodiamonds, and Combined Superstructures. *Chem. Rev.* **2015**, *115*, 4744–4822. [CrossRef]
3. Ding, H.; Li, X.H.; Chen, X.B.; Wei, J.S.; Li, X.B.; Xiong, H.M. Surface states of carbon dots and their influences on luminescence. *J. Appl. Phys.* **2020**, *127*, 231101. [CrossRef]
4. Meng, X.; Wang, M.; Lin, J.; Wang, L.; Liu, J.; Song, Y.; Jing, Q.; Zhao, H. Intermediate aminophenol enables hectogram-scale synthesis of highly bright red carbon quantum dots under ambient conditions. *Chem. Sci.* **2024**, *15*, 9806–9813. [CrossRef]
5. Lin, J.; Wang, L.; Jing, Q.; Zhao, H. Highly efficient and high color rendering index multilayer luminescent solar concentrators based on colloidal carbon quantum dots. *Chem. Eng. J.* **2024**, *481*, 148441. [CrossRef]
6. Wang, L.; Liu, G.; Wang, M.; Song, Y.; Jing, Q.; Zhao, H. Vacuum-Boosting Precise Synthetic Control of Highly Bright Solid-State Carbon Quantum Dots Enables Efficient Light Emitting Diodes. *Small* **2024**, *20*, 2401812. [CrossRef] [PubMed]
7. Zhang, Y.Y.; Chen, S.; Xiang, H.; Gong, X.G. Hybrid crystalline sp23 carbon as a high-efficiency solar cell absorber. *Carbon* **2016**, *109*, 246–252. [CrossRef]
8. Qureshi, Z.A.; Dabash, H.; Ponnamma, D.; Abbas, M.K.G. Carbon dots as versatile nanomaterials in sensing and imaging: Efficiency and beyond. *Heliyon* **2024**, *10*, e31634. [CrossRef]
9. Varma, R.S. Biomass-Derived Renewable Carbonaceous Materials for Sustainable Chemical and Environmental Applications. *ACS Sustain. Chem. Eng.* **2019**, *7*, 6458–6470. [CrossRef]
10. Lesani, P.; Mohamad Hadi, A.H.; Lu, Z.; Palomba, S.; New, E.J.; Zreiqat, H. Design principles and biological applications of red-emissive two-photon carbon dots. *Commun. Mater.* **2021**, *2*, 108. [CrossRef]
11. Ullah, M.; Awan, U.A.; Ali, H.; Wahab, A.; Khan, S.U.; Naeem, M.; Ruslin, M.; Mustopa, A.Z.; Hasan, N. Carbon Dots: New Rising Stars in the Carbon Family for Diagnosis and Biomedical Applications. *J. Nanotheranostics* **2024**, *6*, 1. [CrossRef]
12. Zuo, P.; Lu, X.; Sun, Z.; Guo, Y.; He, H. A review on syntheses, properties, characterization and bioanalytical applications of fluorescent carbon dots. *Microchim. Acta* **2016**, *183*, 519–542. [CrossRef]

13. Aksu, M.; Güzdemir, Ö. Food Waste-Derived Carbon Quantum Dots and Their Applications in Food Technology: A Critical Review. *Food Bioprocess Technol.* **2025**, *18*, 6753–6778. [CrossRef]
14. De Matteis, V.; Rizzello, L.; Di Bello, M.P.; Rinaldi, R. One-step synthesis, toxicity assessment and degradation in tumoral pH environment of SiO_2@Ag core/shell nanoparticles. *J. Nanopart. Res.* **2017**, *19*, 14. [CrossRef]
15. Lvov, Y.; Abdullayev, E. Functional polymer–clay nanotube composites with sustained release of chemical agents. *Prog. Polym. Sci.* **2013**, *38*, 1690–1719. [CrossRef]
16. Adeyemi, J.O.; Oriola, A.O.; Onwudiwe, D.C.; Oyedeji, A.O. Plant Extracts Mediated Metal-Based Nanoparticles: Synthesis and Biological Applications. *Biomolecules* **2022**, *12*, 627. [CrossRef]
17. De Matteis, V.; Rizzello, L.; Ingrosso, C.; Rinaldi, R. Purification of olive mill wastewater through noble metal nanoparticle synthesis: Waste safe disposal and nanomaterial impact on healthy hepatic cell mitochondria. *Environ. Sci. Pollut. Res.* **2021**, *28*, 26154–26171. [CrossRef] [PubMed]
18. Awada, F.; Hamade, K.; Kassir, M.; Hammoud, Z.; Mesnard, F.; Rammal, H.; Fliniaux, O. Laurus nobilis Leaves and Fruits: A Review of Metabolite Composition and Interest in Human Health. *Appl. Sci.* **2023**, *13*, 4606. [CrossRef]
19. Venugopalan, P.; Vidya, N. Microwave-Assisted Green Synthesis of Carbon Dots Derived from Wild Lemon (*Citrus pennivesiculata*) Leaves as a Fluorescent Probe for Tetracycline Sensing in Water. Spectrochim. *Acta A Mol. Biomol. Spectrosc.* **2023**, *286*, 122024. [CrossRef] [PubMed]
20. Suhail, B.; Bajpai, S.K.; Souza, A.D. Microwave-assisted facile green synthesis of carrageenan carbon dots (CDs) and their interaction with Hibiscus Rosa sinensis leaf cells. *Int. J. Environ. Anal. Chem.* **2022**, *102*, 2697–2713. [CrossRef]
21. Sharma, N.; Sharma, I.; Bera, M.K. Microwave-Assisted Green Synthesis of Carbon Quantum Dots Derived from Calotropis gigantea as a Fluorescent Probe for Bioimaging. *J. Fluoresc.* **2022**, *32*, 1039–1049. [CrossRef]
22. Yu, T.; Wang, H.; Guo, C.; Zhai, Y.; Yang, J.; Yuan, J. A Rapid Microwave Synthesis of Green-Emissive Carbon Dots with Solid-State Fluorescence and pH-Sensitive Properties. *R. Soc. Open Sci.* **2018**, *5*, 180245. [CrossRef]
23. Liu, L.; Mi, Z.; Hu, Q.; Li, C.; Li, X.; Feng, F. Green Synthesis of Fluorescent Carbon Dots as an Effective Fluorescence Probe for Morin Detection. *Anal. Methods* **2019**, *11*, 353–358. [CrossRef]
24. Architha, N.; Ragupathi, M.; Shobana, C.; Selvankumar, T.; Kumar, P.; Lee, Y.S.; Kalai Selvan, R. Microwave-Assisted Green Synthesis of Fluorescent Carbon Quantum Dots from Mexican Mint Extract for Fe^{3+} Detection and Bio-Imaging Applications. *Environ. Res.* **2021**, *199*, 111263. [CrossRef] [PubMed]
25. Liu, M.; Zhu, G.; Tian, Y. The historical evolution and research trends of life cycle assessment. *Green Carbon* **2024**, *2*, 425–437. [CrossRef]
26. Piccinno, F.; Hischier, R.; Seeger, S.; Som, C. From laboratory to industrial scale: A scale-up framework for chemical processes in life cycle assessment studies. *J. Clean. Prod.* **2016**, *135*, 1085–1097. [CrossRef]
27. SimaPro 10.2, PRé Sustainability, Stationsplein 121, 3818; Amersfoort, The Netherlands. Available online: https://simapro.com/ (accessed on 24 August 2025).
28. *ISO 14044:2006*; Environmental Management—Life Cycle Assessment—Requirements and Guidelines. International Organization for Standardization: Geneva, Switzerland, 2006.
29. Sharma, A.; Das, J. Small molecules derived carbon dots: Synthesis and applications in sensing, catalysis, imaging, and biomedicine. *J. Nanobiotechnol.* **2019**, *17*, 92. [CrossRef]
30. Lakowicz, J.R. (Ed.) *Principles of Fluorescence Spectroscopy*; Springer: New York, NY, USA, 2007; ISBN 978-0-387-46312-4.
31. Baker, S.N.; Baker, G.A. Luminescent carbon nanodots: Emergent nanolights. *Angew. Chem. Int. Ed.* **2010**, *49*, 6726–6744. [CrossRef]
32. Li, H.; Kang, Z.; Liu, Y.; Lee, S.T. Carbon nanodots: Synthesis, properties and applications. *J. Mater. Chem.* **2012**, *22*, 24230–24253. [CrossRef]
33. Miao, P.; Han, K.; Tang, Y.; Wang, B.; Lin, T.; Cheng, W. Recent advances in carbon nanodots: Synthesis, properties and biomedical applications. *Nanoscale* **2015**, *7*, 1586–1595. [CrossRef]
34. Binderbauer, P.J.; Woegerbauer, M.; Nagovnak, P.; Kienberger, T. The effect of "energy of scale" on the energy consumption in different industrial sectors. *Sustain. Prod. Consum.* **2023**, *41*, 75–87. [CrossRef]